 Bull. Chem. Soc. Jpn. Vol. 82, No. 12, 1497–1505 (2009)

Mononuclear Bis(tridentate)-Type and Dinuclear Triple Helicate Iron(II) Complexes Containing 2-Ethyl-5-methylimidazole-4-carbaldehyde Azine

Yukinari Sunatsuki,*[1] Hisashi Maruyama,[1] Kunihiro Fujita,[1] Takayoshi Suzuki,[1] Masaaki Kojima,*[1] and Naohide Matsumoto[2]

[1]Department of Chemistry, Faculty of Science, Okayama University, 3-1-1 Tsushima-naka, Okayama 700-8530

[2]Faculty of Science, Kumamoto University, 2-39-1 Kurokami, Kumamoto 860-8555

Received June 15, 2009; E-mail: kojima@cc.okayama-u.ac.jp

Mononuclear $[Fe(H_2L^{2\text{-Et-5-Me}})_2]^{2+}$ and dinuclear $[Fe_2(H_2L^{2\text{-Et-5-Me}})_3]^{4+}$ complexes, where $H_2L^{2\text{-Et-5-Me}}$ denotes 2-ethyl-5-methylimidazole-4-carbaldehyde azine, were prepared and isolated as the perchlorate salts, and their structures and magnetic properties were studied. In the mononuclear complex, the ligand acts as an unsymmetrical tridentate ligand with two imidazole nitrogen atoms and one azine nitrogen atom. The complex was in the HS state above 50 K. In the dinuclear complex, each ligand acts as a dinucleating ligand employing four nitrogen atoms to form a triple helicate structure. Two types of crystals, plates and blocks, were isolated for the dinuclear complex. The plate crystals exhibited a sharp spin transition, [LS–HS] ↔ [HS–HS], with no [LS–LS] state being observed. The block crystals remained in the [HS–HS] state above 50 K.

The phenomenon of spin crossover (SCO) is a spectacular example of molecular bistability. SCO can be brought about not only by variation in temperature but also by other external perturbations such as variation in the pressure, or by counter ions or even solvent molecule exchange, light irradiation, a magnetic field, or soft or hard X-ray irradiation.[1] Much attention is being paid to SCO because it can be used to produce molecular memories and switches in electronic devices.[2]

As early as 1958, Busch and Stratton reported that the pyridine-2-carbaldehyde azine ligand, PAA (Scheme 1), could form two types of metal complexes, mononuclear $[M(PAA)_2]^{2+}$ (M^{II} = Fe and Ni) and dinuclear $[M_2(PAA)_3]^{4+}$ (Scheme 2).[3] An iron(II) complex having a $3d^6$ electron configuration can exist in two different ground states, the high-spin (HS) and low-spin (LS) states, depending on the magnitude of the ligand-field strength. Both of the iron(II) complexes, $[Fe(PAA)_2]^{2+}$ and $[Fe_2(PAA)_3]^{4+}$, are reported to be in the LS state. Because an imidazole nitrogen atom usually exhibits a weaker ligand-field strength than a pyridine nitrogen atom exhibits, we expected that the imidazole analog of PAA, imidazole-4-carbaldehyde azine (=H_2L^H, Scheme 1), would have the necessary ligand-field strength to form SCO Fe^{II} complexes. The incorporation of imidazole groups has another advantage because the uncoordinated NH groups can be involved in hydrogen-bond formation to increase cooperativity. For example, we have reported that Fe complexes with a tripodal ligand involving three imidazole groups have a 2-dimensional (2-D) extended network structure based on imidazole–imidazolate hydrogen bonds and that they exhibit steep and multistep SCO behavior.[4]

Switching from PAA to H_2L^H, we were able to obtain the SCO dinuclear triple helicate complex, $[Fe_2(H_2L^H)_3](ClO_4)_4$.[5] The complex exhibited a sharp spin transition, [LS–HS] ↔ [HS–HS], at ca. 240 K. The 2-methyl derivative of the ligand, $H_2L^{2\text{-Me}}$, also afforded the dinuclear complex, $[Fe_2(H_2L^{2\text{-Me}})_3](ClO_4)_4$. The complex was in the LS state over the 5–300 K

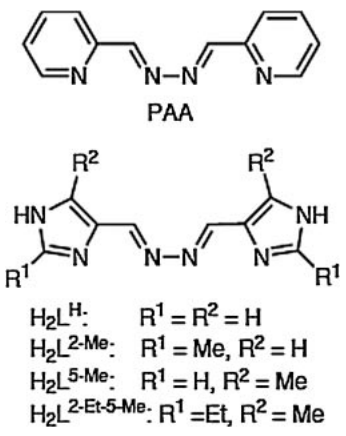

Scheme 1. Ligands, PAA, H_2L^H, $H_2L^{2\text{-Me}}$, $H_2L^{5\text{-Me}}$, and $H_2L^{2\text{-Et-5-Me}}$.

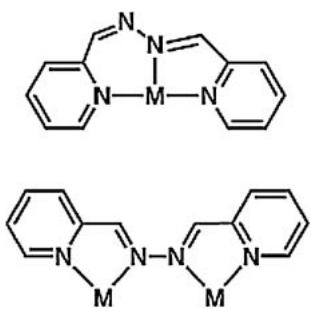

Scheme 2. Two coordination modes adopted by PAA.

Published on the web December 10, 2009; doi:10.1246/bcsj.82.1497

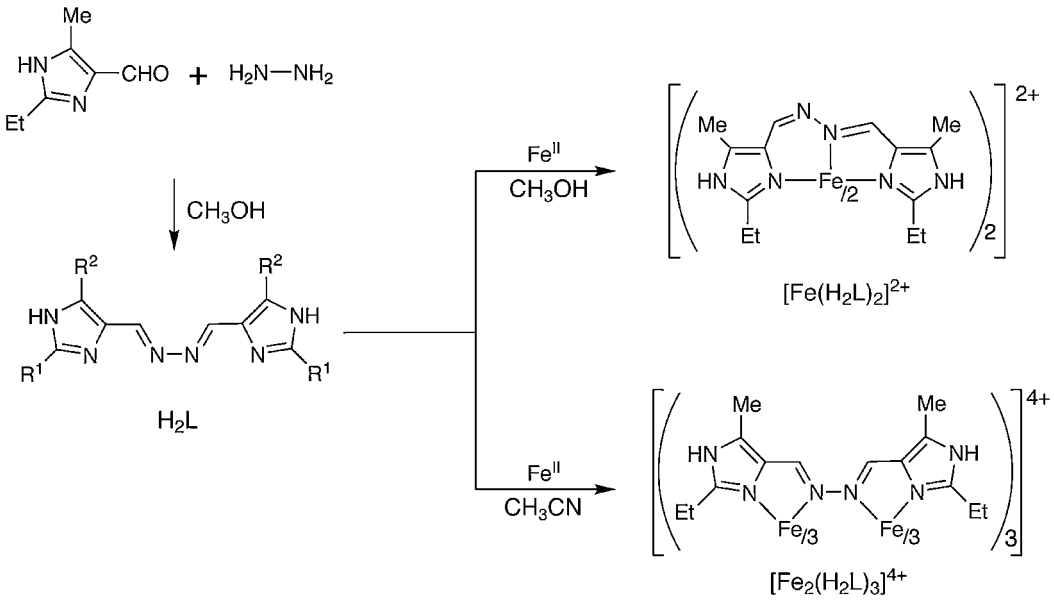

Figure 1. Synthetic procedures yielding the $H_2L^{2\text{-Et-5-Me}}$ ligand and the mononuclear and dinuclear Fe^{II} complexes.

temperature range, and the ligand-field strength of $H_2L^{2\text{-Me}}$ with electron-donating methyl groups was greater than that of H_2L^{H}, in accordance with our expectation. The spin states were retained in solution.

However, in the mononuclear $[Fe(H_2L^{H})_2](ClO_4)_2$ and $[Fe(H_2L^{2\text{-Me}})_2](ClO_4)_2$ complexes, a different order of ligand-field strengths, $H_2L^{H} > H_2L^{2\text{-Me}}$, was observed because $[Fe(H_2L^{H})_2](ClO_4)_2$ was in the LS state while $[Fe(H_2L^{2\text{-Me}})_2](ClO_4)_2$ was in the HS state at room temperature, both in the solid state and in solution.[5] This unexpected result was explained in terms of interligand steric repulsion between a methyl group of an $H_2L^{2\text{-Me}}$ ligand and the other ligand in $[Fe(H_2L^{2\text{-Me}})_2]^{2+}$. In this case, the steric effect outweighs the electron-donating effect of the methyl group. The $[Fe(H_2L^{5\text{-Me}})_2](ClO_4)_2$ complex does not involve such a steric congestion, and the complex stayed in the LS state over the 5–300 K temperature range.

Here we report the synthesis, characterization, structure, and magnetic properties of the mononuclear $[Fe(H_2L^{2\text{-Et-5-Me}})_2]^{2+}$ and the dinuclear $[Fe_2(H_2L^{2\text{-Et-5-Me}})_3]^{4+}$ complexes, where $H_2L^{2\text{-Et-5-Me}}$ denotes 2-ethyl-5-methylimidazole-4-carbaldehyde azine. Because the ligand involves two electron-donating groups on each imidazole moiety, it is interesting to examine how the substituents affect the spin states of the complexes.

Results and Discussion

Synthesis and Characterization. The synthetic procedures yielding the $H_2L^{2\text{-Et-5-Me}}$ ligand and the Fe^{II} complexes are shown schematically in Figure 1. The ligand was prepared by condensation of 2-ethyl-4-methyl-5-formylimidazole with hydrazine in a 2:1 mol ratio in methanol. The red mononuclear complex with the $H_2L^{2\text{-Et-5-Me}}$ ligand, $[Fe(H_2L^{2\text{-Et-5-Me}})_2](ClO_4)_2\cdot CH_3OH$ (**1**), was prepared by the reaction of $H_2L^{2\text{-Et-5-Me}}$ and $Fe(ClO_4)_2\cdot 6H_2O$ in a 2:1 mol ratio in methanol. The perchlorate of the dinuclear $[Fe_2(H_2L^{2\text{-Et-5-Me}})_3]^{4+}$ complex was prepared by the reaction of the ligand and $Fe(ClO_4)_2\cdot 6H_2O$ in a 3:2 mol ratio in acetonitrile. The yellow product was a mixture of plate crystals, $[Fe_2(H_2L^{2\text{-Et-5-Me}})_3](ClO_4)_4\cdot 0.5H_2O\cdot 3CH_3CN$ (**2-plate**), and block crystals, $[Fe_2(H_2L^{2\text{-Et-5-Me}})_3](ClO_4)_4\cdot 2CH_3CN$ (**2-block**). They were separated manually under a microscope. The dinuclear complex is stable only in such solvents as nitromethane and acetonitrile. Crystals of **2-plate** used for the X-ray diffraction study involved three acetonitrile molecules in addition to one half water molecule as crystal solvents, but the acetonitrile molecules were easily lost on standing in air, and such samples, $[Fe_2(H_2L^{2\text{-Et-5-Me}})_3](ClO_4)_4\cdot H_2O$ (**2-plate′**), were used for measurements other than the X-ray analysis. The **2-block** complex also loses some acetonitrile molecules, and the sample we used for the magnetic study had the formula $[Fe_2(H_2L^{2\text{-Et-5-Me}})_3](ClO_4)_4\cdot 0.5CH_3CN$ (**2-block′**).

The IR spectrum of the free $H_2L^{2\text{-Et-5-Me}}$ ligand showed a strong characteristic absorption at 1625 cm^{-1}, assignable to the C=N stretching vibration.[6] The dinuclear complexes showed one ν(C=N) band at 1628 cm^{-1}, while the mononuclear complex showed two bands at 1559 cm^{-1} and at ca. 1634 cm^{-1}. The number of ν(C=N) bands, one for the dinuclear complexes and two for the mononuclear complex, is in accordance with the symmetry of the complexes, because in the mononuclear complex, the $H_2L^{2\text{-Et-5-Me}}$ ligand functions as an unsymmetrical tridentate ligand, and the two imine moieties are nonequivalent. The electron density on the C=N moiety is donated to a metal upon coordination, and the double-bond character decreases, so that the position of the ν(C=N) band should shift to the lower wavenumber region. Thus, the band in the lower wavenumber region of the mononuclear complex (1559 cm^{-1}) can be assigned to the coordinated C=N moiety. The band in the higher wavenumber region (1634 cm^{-1}) was observed near to that of the free ligand (1625 cm^{-1}), and it can be safely assigned to the uncoordinated C=N moiety.

The UV–vis spectra of the mononuclear (**1**) and the dinuclear (**2**) complexes in acetonitrile are shown in Figure 2. Both complexes have an intense absorption band attributable to the metal-to-ligand charge-transfer transition in the visible

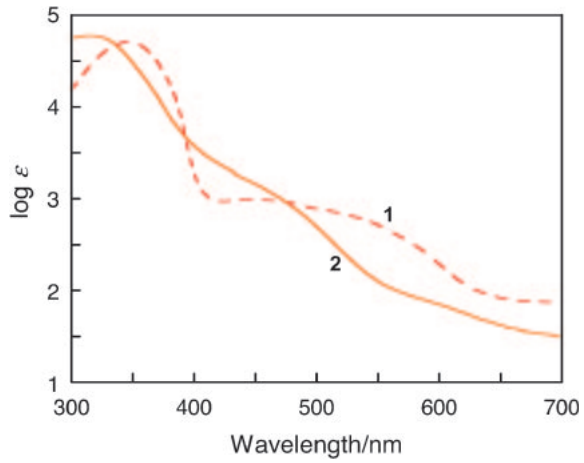

Figure 2. UV–vis spectra for the mononuclear $[Fe(H_2L^{2\text{-Et-5-Me}})_2](ClO_4)_2$ (**1**, ---) and dinuclear $[Fe_2(H_2L^{2\text{-Et-5-Me}})_3](ClO_4)_4$ (**2**, —) complexes in acetonitrile.

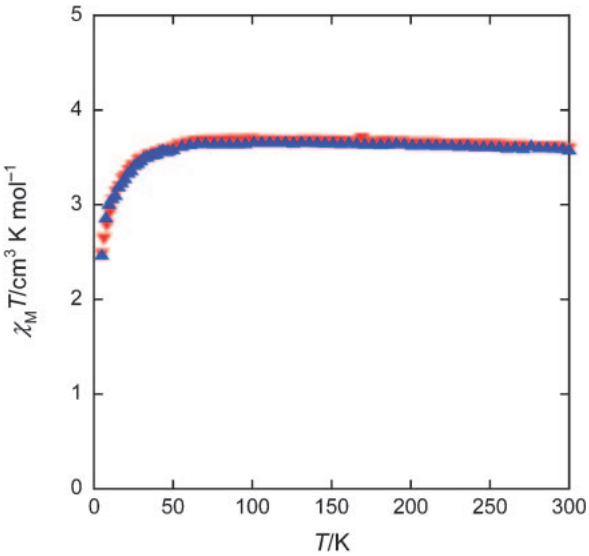

Figure 3. Magnetic behavior of $[Fe(H_2L^{2\text{-Et-5-Me}})_2](ClO_4)_2 \cdot CH_3OH$ (**1**, ▲ and ▼) in the form of $\chi_M T$ versus T plots. The sample was quickly cooled from 300 to 5 K and χ_M was successively measured in the heating (5–300 K, ▲) and cooling (300–5 K, ▼) modes, at a sweep rate of 2 K min^{-1}.

region,[7] which is responsible for the deep color, and thus weak d–d bands are obscured. Both complexes have an intense band at 315–350 nm assignable to the imine π–π^* transition of the ligands.[8]

Magnetic Properties of the Mononuclear Complex. The magnetic behavior of $[Fe(H_2L^{2\text{-Et-5-Me}})_2](ClO_4)_2 \cdot CH_3OH$ (**1**) is shown in Figure 3 in the form of $\chi_M T$ versus T plots, where χ_M is the molar magnetic susceptibility and T is the absolute temperature. Complex **1** remains in the HS state above 50 K. The $\chi_M T$ value of 3.65 cm^3 K mol^{-1} at 300 K is within the range of expected values for a paramagnetic Fe^{II} in its HS state with some orbital contribution. The drop in $\chi_M T$ below 50 K may be due to the zero-field splitting (ZFS) of Fe^{II} in the HS state. We have shown in a previous paper that the mononuclear iron(II) complex of H_2L^H, $[Fe(H_2L^H)_2]^{2+}$, is in the LS state

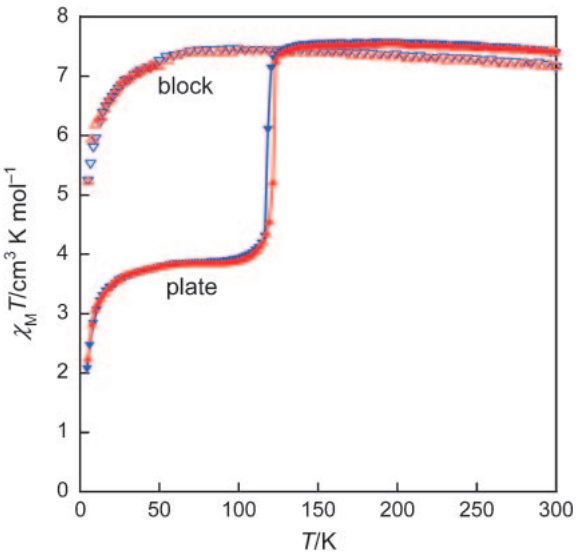

Figure 4. Magnetic behavior of $[Fe_2(H_2L^{2\text{-Et-5-Me}})_3](ClO_4)_4 \cdot H_2O$ (**2-plate′**, ▲ and ▼) and $[Fe_2(H_2L^{2\text{-Et-5-Me}})_3](ClO_4)_4 \cdot 0.5CH_3CN$ (**2-block′**, △ and ▽) in the form of $\chi_M T$ versus T plots.

while the complex with $H_2L^{2\text{-Me}}$ ligands, $[Fe(H_2L^{2\text{-Me}})_2]^{2+}$, remains in the HS state in the 50–300 K range, and the results were explained in terms of the intramolecular steric effect.[5] It should be noted that the difference in the spin states was also observed in solution, as evidenced by the UV–vis spectra. The fact that **1** is in the HS state above 50 K shows that the steric effect outweighs the electronic effect; we discuss this feature in more detail in the section on the X-ray structures. A substituent effect on the spin equilibrium has also been observed for Fe^{II} complexes with hexadentate ligands.[9]

Magnetic Properties of the Dinuclear Complexes. In a previous paper, we studied the magnetic properties of the related dinuclear complexes, $[Fe_2(H_2L^H)_3]X_4$ and $[Fe_2(H_2L^{2\text{-Me}})_3]X_4$ ($X^- = ClO_4^-$ and BF_4^-).[5] $[Fe_2(H_2L^H)_3]X_4$ showed an SCO behavior between the [LS–HS] and [HS–HS] states. On the other hand, $[Fe_2(H_2L^{2\text{-Me}})_3]X_4$, involving electron-donating methyl groups on the ligand, did not show an SCO and stayed in the [LS–LS] state in the 5–300 K range. These results were explained in terms of the electronic effect of the substituent (H or CH_3) on the ligand. Thus, we expected that the $H_2L^{2\text{-Et-5-Me}}$ ligand is not suited for constructing SCO complexes because the ligand has two electron-donating groups on each imidazole ring and the magnitude of the ligand-field strength is too large to cause SCO. In reality, the dinuclear $[Fe_2(H_2L^{2\text{-Et-5-Me}})_3]^{4+}$ complexes have a ligand-field strength at around the SCO point.

As described above, **2** was obtained in two crystal forms, plates and blocks. The magnetic behaviors of $[Fe_2(H_2L^{2\text{-Et-5-Me}})_3](ClO_4)_4 \cdot H_2O$ (**2-plate′**) and $[Fe_2(H_2L^{2\text{-Et-5-Me}})_3](ClO_4)_4 \cdot 0.5CH_3CN$ (**2-block′**) are shown in Figure 4 in the form of a $\chi_M T$ versus T plot. The block crystals (**2-block′**) stayed in the HS state at least above 50 K, and the profile suggests that the magnetic interaction between the Fe sites would be quite small. The plate crystals (**2-plate′**) exhibited an abrupt spin transition at ca. 120 K (Figure 4). Above 125 K, the $\chi_M T$ value was nearly constant at 7.53 cm^3 K mol^{-1}, which is

Table 1. X-ray Crystallographic Data for $H_2L^{2\text{-Et-5-Me}}$, $[Fe(H_2L^{2\text{-Et-5-Me}})_2](ClO_4)_2\cdot CH_3OH$ (**1**), $[Fe_2(H_2L^{2\text{-Et-5-Me}})_3](ClO_4)_4\cdot 2CH_3CN$ (**2-block**), and $[Fe_2(H_2L^{2\text{-Et-5-Me}})_3](ClO_4)_4\cdot 0.5H_2O\cdot 3CH_3CN$ (**2-plate**)

	$H_2L^{2\text{-Et-5-Me}}$	**1**	**2-block**	**2-plate**
Formula	$C_{14}H_{20}N_6$	$C_{29}H_{44}Cl_2FeN_{12}O_9$	$C_{46}H_{66}Cl_4Fe_2N_{20}O_{16}$	$C_{96}H_{140}Cl_8Fe_4N_{42}O_{33}$
Formula weight	272.35	831.49	1408.66	2917.44
Crystal system	monoclinic	orthorhombic	orthorhombic	orthorhombic
Space group	$P2_1/a$ (No. 14)	$P2_12_12_1$ (No. 19)	$Pca2_1$ (No. 29)	$Pbca$ (No. 61)
a/Å	9.242(2)	12.3001(6)	16.6701(4)	15.4434(5)
b/Å	8.3388(19)	17.2610(9)	17.6058(5)	21.1318(8)
c/Å	10.186(2)	36.6951(15)	21.3414(6)	41.4394(14)
α/°	90	90	90	90
β/°	97.241(6)	90	90	90
γ/°	90	90	90	90
V/Å^3	778.7(3)	7790.8(6)	6263.5(3)	13523.6(8)
T/K	193	193	113	163
Z	2	8	4	4
D_{calcd}/g cm^{-3}	1.161	1.418	1.494	1.433
μ/cm^{-1}	0.748	5.877	7.128	6.649
R_1[a] [$I > 2\sigma(I)$]	0.0557	0.0684	0.0407	0.0787
wR_2[b] [all data]	0.1775	0.2111	0.1115	0.2369

a) $R_1 = \Sigma||F_o| - |F_c||/\Sigma|F_o|$. b) $wR_2 = [\Sigma w(|F_o^2| - |F_c^2|)^2/\Sigma w|F_o^2|^2]^{1/2}$.

larger than the calculated spin-only value for the [HS–HS] system ($\chi_M T = 6.0\,cm^3\,K\,mol^{-1}$) but in the range of the [HS–HS] systems reported so far.[10] In the temperature range 50–100 K, the value of $\chi_M T$ was nearly constant at $3.85\,cm^3\,K\,mol^{-1}$, indicating that 50% of the Fe^{II} sites were in the HS state. The half-SCO state was trapped and the complex was locked into it, and it did not change into the [LS–LS] state on further reducing the temperature. The decrease in $\chi_M T$ observed below ca. 50 K is probably due to the ZFS effect. Three different spin-pair states are possible in diiron(II) complexes: [LS–LS], [LS–HS], and [HS–HS]. Actually, some complexes exhibit a two-step SCO phenomenon, [LS–LS] ↔ "[LS–HS]" ↔ [HS–HS].[11] The half-SCO species, "[LS–HS]," can consist of either a 1:1 mixture of [LS–LS] and [HS–HS] complexes or a distinct [LS–HS] complex. Kaizaki and co-workers reported that the "[LS–HS]" species of their doubly pyrazolate-bridged two-step SCO diiron(II) complex is a mixture of [LS–LS] and [HS–HS] complexes.[11f] Recently, Murray and co-workers confirmed for the first time the existence of the mixed-spin state [LS–HS] from X-ray crystallographic data of the doubly 1,2,4-triazole-bridged complex.[12] Amoore et al. structurally characterized the three spin states, [LS–LS], [LS–HS], and [HS–HS], for the first time.[11g]

The X-ray crystal structure analysis verified that the half-SCO species of **2-plate** assumes a mixed-spin state, [LS–HS] (see below). The correlation between the structure and magnetic properties of the two forms of **2** is discussed in the section on X-ray structures.

X-ray Crystal Structures. Structure of the $H_2L^{2\text{-Et-5-Me}}$ Ligand: Crystals of $H_2L^{2\text{-Et-5-Me}}$ suitable for an X-ray crystal structure analysis were grown from a methanol solution. The ligand crystallizes in the space group $P2_1/a$ (No. 14) with $Z = 2$. The crystallographic data are collated in Table 1, and selected bond lengths and angles are listed in Table S1. Figure 5 shows the molecular structure with an atom numbering scheme. There is a crystallographic inversion center at the midpoint of N3 and N3*. The molecule is the E–E isomer. The

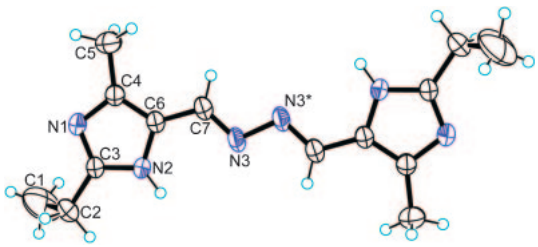

Figure 5. ORTEP drawing of the $H_2L^{2\text{-Et-5-Me}}$ ligand with atom numbering scheme showing 50% probability ellipsoids. Symmetry operator *: $-x + 1$, $-y$, $-z + 1$.

nitrogen–nitrogen bond N3–N3* (1.4057(18) Å, *: $-x + 1$, $-y$, $-z + 1$) can be formally defined as a single bond but shorter than the N–N bond in hydrazine (1.45 Å). The C–N bond C7–N3 (1.284(2) Å) is considered to have full double-bond character. N2 rather than N1 is protonated. Obviously, upon coordination, the proton is transferred from N2 to N1. Figure S1 shows the packing diagram as viewed down the *ab*-plane. Imidazole N2–H6 is hydrogen bonded to N1 of the neighboring molecule, N2–H6···N1** (N2···N1** = 2.9053(16) Å, **: $-1/2 + x$, $1/2 - y$, $+z$), to form a 2-D sheet structure in the *ab*-plane.

Structure of $[Fe(H_2L^{2\text{-Et-5-Me}})_2](ClO_4)_2\cdot CH_3OH$ (1): The crystal structure of **1** was determined at 193 K. The asymmetric unit consists of two $[Fe(H_2L^{2\text{-Et-5-Me}})_2]^{2+}$ cations, four ClO_4^- anions, and two methanol molecules. The molecular structure of **1** is shown in Figure 6. Each Fe^{II} ion binds two $H_2L^{2\text{-Et-5-Me}}$ ligands and has a pseudo-octahedral coordination geometry. Each ligand in the Z–E form serves as a tridentate ligand and coordinates meridionally to the metal ion with two imidazole nitrogen atoms and one azine nitrogen atom, and the other azine nitrogen atom remains uncoordinated (Figure 1). Thus, the $H_2L^{2\text{-Et-5-Me}}$ ligand becomes unsymmetrical upon coordination to form a five-membered and a six-membered chelate. This creates disorder in the moieties involving azine. In the complex containing Fe1, the occupancy (Occ) values for

C21–N9–N10–C22 and C23–N11–N12–C24 were 0.60 and 0.40, respectively, and in the other complex containing Fe2, the Occ values for C37–N17–N18–C38, C39–N19–N20–C40, C53–N25–N26–C54, and C55–N27–N28–C56 were 0.64, 0.36, 0.50, and 0.50, respectively. Selected bond lengths and angles are listed in Table 2. All of the Fe–N coordinate bond lengths (2.142(5)–2.246(15) Å) are typical for HS Fe^{II},[13] in agreement with the magnetic study. The crystal structure is shown in Figure S2. Four imidazole hydrogen atoms, N1–H6, N6–H15, N7–H26, and N14–H37 of the complex involving Fe1, are linked to O10, O17, and O9 of ClO_4^-, and azine N18 of the adjacent cation involving Fe2, respectively, by hydrogen bonds with distances of N1···O10 = 2.951(8), N6···O17 = 2.910(9), N7···O9 = 2.849(9), and N14···N18 = 2.896(7) Å. The imidazole hydrogen atoms, N15–H48, N22–H59, N23–H70, and N30–H81 of the complex involving Fe2, are linked to O1, O7, O4, and O12 of ClO_4^-, by hydrogen bonds with distances of N15···O1 = 2.764(9), N22···O7 = 2.832(9), N23···O4 = 3.059(12), and N30···O12 = 2.890(9) Å. A three-dimensional (3-D) structure is formed by these hydrogen bonds.

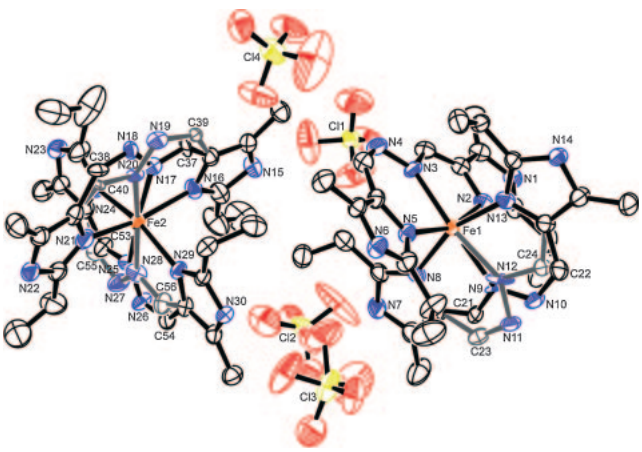

Figure 6. Molecular structure of $[Fe(H_2L^{2\text{-Et-5-Me}})_2](ClO_4)_2 \cdot CH_3OH$ (**1**) with an atom numbering scheme showing the 30% probability ellipsoids. The hydrogen atoms and methanol molecule have been omitted for clarity. Color code: orange: HS Fe, blue: N, black: C, yellow: Cl, and red: O. The structure suffers from disorder at the azine moieties and perchlorate ions (Cl2 and Cl3).

Figure 7 compares the intramolecular steric interaction in **1** and $[Fe(H_2L^{H})_2](ClO_4)_2 \cdot 2CH_3CN$. In Figure 7, one of the ligands of each complex cation is in the plane of the paper, and the other ligand is perpendicular to the paper. The N2–Fe1–N7 bond of $[Fe(H_2L^{H})_2](ClO_4)_2 \cdot 2CH_3CN$ is almost linear

Table 2. Relevant Bond Lengths (Å) and Angles (°) with Their Estimated Standard Deviations in Parentheses for $[Fe(H_2L^{2\text{-Et-5-Me}})_2](ClO_4)_2 \cdot CH_3OH$ (**1**)

Bond distances/Å			
Fe1–N2	2.244(4)	Fe1–N3	2.205(4)
Fe1–N5	2.162(4)	Fe1–N8	2.158(4)
Fe1–N9	2.237(7)	Fe1–N12	2.147(17)
Fe1–N13	2.168(3)		
Fe2–N16	2.159(4)	Fe2–N17	2.240(10)
Fe2–N20	2.246(15)	Fe2–N21	2.142(5)
Fe2–N24	2.177(4)	Fe2–N25	2.235(14)
Fe2–N28	2.165(18)	Fe2–N29	2.167(4)
Bond angles/°			
N2–Fe1–N3	76.60(17)	N2–Fe1–N5	160.89(16)
N2–Fe1–N8	89.54(16)	N2–Fe1–N9	89.4(2)
N2–Fe1–N12	95.6(4)	N2–Fe1–N13	91.04(14)
N3–Fe1–N5	84.33(16)	N3–Fe1–N8	97.79(17)
N3–Fe1–N9	164.2(3)	N3–Fe1–N12	170.0(4)
N3–Fe1–N13	101.79(16)	N5–Fe1–N8	94.44(16)
N5–Fe1–N9	109.7(2)	N5–Fe1–N12	103.2(4)
N5–Fe1–N13	91.53(15)	N8–Fe1–N9	74.6(3)
N8–Fe1–N12	88.3(5)	N8–Fe1–N13	160.00(18)
N9–Fe1–N13	85.4(3)	N12–Fe1–N13	71.7(5)
N16–Fe2–N17	72.2(4)	N16–Fe2–N20	89.6(7)
N16–Fe2–N21	160.07(19)	N16–Fe2–N24	93.48(19)
N16–Fe2–N25	97.4(4)	N16–Fe2–N28	99.5(5)
N16–Fe2–N29	88.74(18)	N17–Fe2–N21	88.2(4)
N17–Fe2–N24	100.4(3)	N17–Fe2–N25	168.0(6)
N17–Fe2–N28	168.9(5)	N17–Fe2–N29	99.1(3)
N20–Fe2–N21	70.7(7)	N20–Fe2–N24	100.9(4)
N20–Fe2–N25	171.3(6)	N20–Fe2–N28	167.5(8)
N20–Fe2–N29	98.9(4)	N21–Fe2–N24	93.61(18)
N21–Fe2–N25	102.4(4)	N21–Fe2–N28	99.5(4)
N21–Fe2–N29	90.89(17)	N24–Fe2–N25	73.7(4)
N24–Fe2–N28	87.1(5)	N24–Fe2–N29	160.10(17)
N25–Fe2–N29	86.4(4)	N28–Fe2–N29	73.0(5)

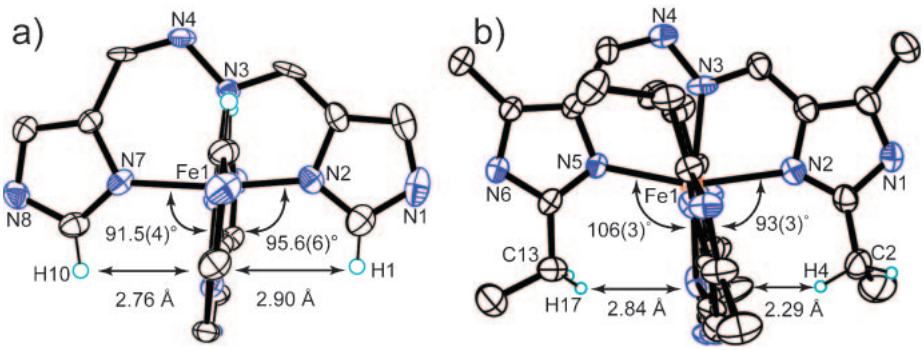

Figure 7. Comparison of the intramolecular steric interactions in (a) $[Fe(H_2L^{H})_2](ClO_4)_2 \cdot 2CH_3CN$ and (b) $[Fe(H_2L^{2\text{-Et-5-Me}})_2](ClO_4)_2 \cdot CH_3OH$ (**1**). Severe steric repulsion exists between an ethyl group of an $H_2L^{2\text{-Et-5-Me}}$ ligand and the other $H_2L^{2\text{-Et-5-Me}}$ ligand in **1**.

(172.71(9)°), while the corresponding bond of **1** is bent (160.89(16)°), and the latter is attributable to the steric effect of the ethyl group. The least-squares plane (P_L) of the $H_2L^{2\text{-Et-5-Me}}$ ligand (or the H_2L^{H} ligand), which is perpendicular to the paper, and the angles between P_L and Fe1–N2, Fe–N5, or Fe1–N7 are defined as in Figure 7. The angle between P_L and Fe1–N5 for **1** (106(3)°) is much larger than that for $[Fe(H_2L^{H})_2](ClO_4)_2\cdot 2CH_3CN$ (91.5(4)°) because of the steric effect. To cope with the steric crowding, the $H_2L^{2\text{-Et-5-Me}}$ ligand tilts and deviates from planarity, as shown by Figure 7b. Such steric crowding will lengthen the Fe–N bond, resulting in the HS state. It is to be noted that $[Fe(H_2L^{H})_2](ClO_4)_2\cdot 2CH_3CN$ is in the LS state while **1**, which contains $H_2L^{2\text{-Et-5-Me}}$ ligands with electron-donating methyl and ethyl groups, is in the HS state. The unusual order in the ligand-field strength, $H_2L^{H} > H_2L^{2\text{-Et-5-Me}}$, in the mononuclear complexes can be accounted for by steric effects.

Structure of $[Fe_2(H_2L^{2\text{-Et-5-Me}})_3](ClO_4)_4\cdot 0.5H_2O\cdot 3CH_3CN$ (2-plate): The X-ray crystal structure analysis was carried out at 163 K. Figure 8 shows the molecular structure of **2-plate** at 163 K, with the atom numbering scheme. Selected bond lengths and angles are collated in Table 3. The Fe1–N bond lengths (2.154(3)–2.210(3) Å) and Fe2–N bond lengths (1.969(3)–2.036(3) Å) are typical for HS Fe^{II} and LS Fe^{II}, respectively.[13] The complex assumes a mixed-spin [LS–HS] state at 163 K, in contrast to the conclusions of the magnetic study. The magnetic study revealed that the complex exhibited an abrupt spin transition at ca. 120 K, and thus we expected the [HS–HS] state at 163 K. This inconsistency seems to be related to the efflorescent nature of the crystals. The acetonitrile molecules involved in the crystals of $[Fe_2(H_2L^{2\text{-Et-5-Me}})_3](ClO_4)_4\cdot 0.5H_2O\cdot 3CH_3CN$ (**2-plate**) are easily lost on standing in air, and the sample thus obtained ($[Fe_2(H_2L^{2\text{-Et-5-Me}})_3](ClO_4)_4\cdot H_2O$ (**2-plate′**)) was used for the magnetic measurements. It has been pointed out that solvent molecules play an important role in the SCO behavior.[1e]

The N(imidazole)–Fe1–N(azine) five-membered chelate angles (74.50(12)–75.03(12)°) are smaller than the N(imidazole)–Fe2–N(azine) angles (79.52(13)–79.80(14)°), and the octahedron is markedly more distorted at the HS Fe1 site than at the LS Fe2 site. The crystal-packing diagrams (Figure S3) of **2-plate** show that all six imidazole N–H groups of a $[Fe_2(H_2L^{2\text{-Et-5-Me}})_3]^{4+}$ complex cation, N1–H6, N7–H26, N12–H35, N13–H46, N18–H55, and N6–H15, are connected to the ClO_4^- anions and acetonitrile molecules by hydrogen

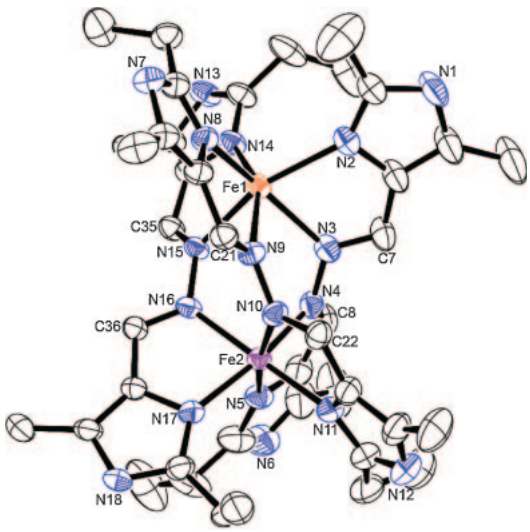

Figure 8. X-ray molecular structure of the cation of $[Fe_2(H_2L^{2\text{-Et-5-Me}})_3](ClO_4)_4\cdot 0.5H_2O\cdot 3CH_3CN$ (**2-plate**) at 163 K with an atom numbering scheme showing the 50% probability ellipsoids. The hydrogen atoms, the ClO_4 anions, and solvent molecules have been omitted for clarity. Color code: purple: LS Fe, orange: HS Fe, blue: N, and black: C.

Table 3. Relevant Bond Lengths (Å) and Angles (°) with Their Estimated Standard Deviations in Parentheses for $[Fe_2(H_2L^{2\text{-Et-5-Me}})_3](ClO_4)_4\cdot 0.5H_2O\cdot 3CH_3CN$ (**2-plate**) at 163 K

	Plate	Block		Plate	Block
Bond distances/Å					
Fe1–N2	2.198(3)	2.126(2)	Fe2–N4	1.969(3)	2.248(2)
Fe1–N3	2.205(3)	2.302(2)	Fe2–N5	2.029(3)	2.157(2)
Fe1–N8	2.156(3)	2.205(2)	Fe2–N10	1.991(3)	2.277(2)
Fe1–N9	2.206(3)	2.208(2)	Fe2–N11	2.036(3)	2.156(2)
Fe1–N14	2.154(3)	2.169(2)	Fe2–N16	1.992(3)	2.220(2)
Fe1–N15	2.210(3)	2.205(2)	Fe2–N17	2.010(3)	2.169(2)
Fe1···Fe2	3.8450(7)	4.1783(4)			
Bond angles/°					
N2–Fe1–N3	74.53(13)	74.01(8)	N4–Fe2–N5	79.80(14)	74.80(8)
N8–Fe1–N9	74.50(12)	74.99(8)	N10–Fe2–N11	79.59(14)	74.64(8)
N14–Fe1–N15	75.03(12)	75.31(8)	N16–Fe2–N17	79.52(13)	75.08(8)
Torsion angles/°					
C7–N3–N4–C8	64.3(5)	85.9(3)			
C21–N9–N10–C22	58.5(5)	66.6(2)			
C35–N15–N16–C36	55.6(5)	77.3(3)			

bonds with distances of N1···O4* = 2.830(11) Å, N7···O6† = 2.844(5) Å, N12···O13‡ = 3.196(10) Å, N12···O14‡ = 2.941(8) Å, N13···O10* = 2.940(4) Å, N18···O10# = 2.844(4) Å, and N6···N20″ = 3.058(15) Å (symmetry codes *: $+x, 1/2-y, 1/2+z$; †: $-1/2+x, +y, 1/2-z$; ‡: $1/2+x, 1/2-y, -z$; #: $1/2+x, +y, 1/2-z$; ″: $1/2-x, -1/2+y, +z$). A one-dimensional network structure is constructed by N13···O10 and N18···O10 hydrogen bonds. Each chain consists of molecules having the same chirality; that is, the Λ–Λ pair chain and the Δ–Δ pair chain coexist in the crystal. The N7···O6, N12···O14, and N6···N20 hydrogen bonds do not participate in the formation of dimensionality.

Structure of $[Fe_2(H_2L^{2\text{-Et-5-Me}})_3](ClO_4)_4\cdot 2CH_3CN$ (2-block) and Comparison with Other Dinuclear Complexes: The X-ray crystal structure analysis of **2-block** was carried out at 113 K. The molecular structure is shown in Figure S4. The Fe–N bond lengths are in the range of 2.126(2)–2.302(2) Å, demonstrating that the complex is in the [HS–HS] state. The crystal-packing diagram (Figure S5) shows that the hydrogen bonds and CH–π interactions form a 3-D structure. Because of these intermolecular interactions, the complex is severely distorted. Figure 9 compares the distortion of the dinuclear complex cations, **2-block**, **2-plate**, $[Fe_2(H_2L^{H})_3](BF_4)_4\cdot 6.5CH_3NO_2\cdot 0.5H_2O$, and $[Fe_2(H_2L^{2\text{-Me}})_3](ClO_4)_4$ as projected down the approximate threefold axis. Uncoordinated imidazole nitrogen atoms of each ligand are connected by red lines. Figure 9 clearly shows that the dinuclear complexes with $H_2L^{2\text{-Et-5-Me}}$ (**2-block** and **2-plate**) have less symmetric structures about the pseudo-C_3 axis of the molecule than those of the related complexes of $[Fe_2(H_2L^{H})_3](BF_4)_4\cdot 6.5CH_3NO_2\cdot 0.5H_2O$, and $[Fe_2(H_2L^{2\text{-Me}})_3](ClO_4)_4$. The average torsion angles around the azine N–N bonds for dinuclear complexes **2** ([LS–HS] state: 60(2)° for **2-plate** and [HS–HS] state: 77(6)° for **2-block**) are larger than those of $[Fe_2(H_2L^{H})_3]X_4$ and $[Fe_2(H_2L^{2\text{-Me}})_3]X_4$ ([LS–HS] state: 56(1)° for $[Fe_2(H_2L^{H})_3](BF_4)_4\cdot 6.5CH_3NO_2\cdot 0.5H_2O$, 57(4)° for $[Fe_2(H_2L^{2\text{-Me}})_3](ClO_4)_4$ at 103 K and [HS–HS] state: 59(4)° for $[Fe_2(H_2L^{2\text{-Me}})_3](ClO_4)_4$ at 293 K). Because of these distortions, the average Fe–N bond lengths of **2** (2.20 Å for the HS site and 2.01 Å for the LS site) are slightly larger than those of $[Fe_2(H_2L^{H})_3](BF_4)_4\cdot 6.5CH_3NO_2\cdot 0.5H_2O$ (2.18 Å for the HS site and 1.98 Å for the LS site). This fact indicates that the electronic effect of the substituent is outweighed by the steric effect and the ligand-field strength of $H_2L^{2\text{-Et-5-Me}}$ is weakened. In the two forms of complex **2**, **2-block** is clearly more distorted from C_3 symmetry, probably because of the hydrogen bonds and CH–π interactions in the crystal structure. Such a distortion lengthens the Fe–N bond, resulting in the HS state being favored.

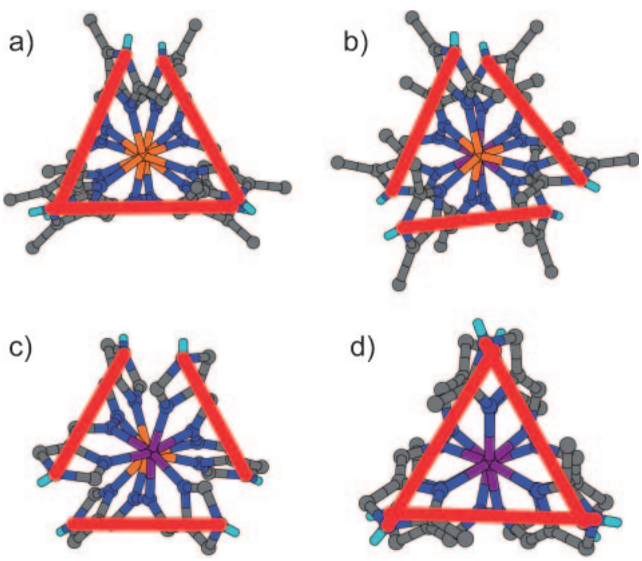

Figure 9. Comparison of the dinuclear complex cations as projected down the approximate threefold axis. (a) $[Fe_2(H_2L^{2\text{-Et-5-Me}})_3](ClO_4)_4\cdot 2CH_3CN$ (**2-block**) at 113 K, (b) $[Fe_2(H_2L^{2\text{-Et-5-Me}})_3](ClO_4)_4\cdot 0.5H_2O\cdot 3CH_3CN$ (**2-plate**), (c) $[Fe_2(H_2L^{H})_3](BF_4)_4\cdot 6.5CH_3NO_2\cdot 0.5H_2O$ at 173 K, and (d) $[Fe_2(H_2L^{2\text{-Me}})_3](ClO_4)_4$ at 293 K. Color code: purple: LS Fe, orange: HS Fe, blue: N, light blue: H, and gray: C.

Conclusion

The $H_2L^{2\text{-Et-5-Me}}$ ligand, 2-ethyl-5-methylimidazole-4-carbaldehyde azine, was prepared by condensation of 2-ethyl-4-methyl-5-formylimidazole with hydrazine in a 2:1 mol ratio in methanol. The ligand afforded mononuclear $[Fe(H_2L^{2\text{-Et-5-Me}})_2]^{2+}$ and dinuclear triple helicate $[Fe_2(H_2L^{2\text{-Et-5-Me}})_3]^{4+}$ complexes, and their magnetic behaviors were compared with each other and with those of $[Fe(H_2L^{H})_2]^{2+}$ and $[Fe_2(H_2L^{H})_3]^{4+}$. Because the $H_2L^{2\text{-Et-5-Me}}$ ligand involves electron-donating methyl and ethyl groups, the order of the ligand-field strength was expected to be $H_2L^{2\text{-Et-5-Me}} > H_2L^{H}$. However, in the mononuclear $[Fe(H_2L^{H})_2](ClO_4)_2$ and $[Fe(H_2L^{2\text{-Et-5-Me}})_2](ClO_4)_2$ complexes, the opposite order, $H_2L^{H} > H_2L^{2\text{-Et-5-Me}}$, was observed because $[Fe(H_2L^{H})_2](ClO_4)_2$ was in the LS state while $[Fe(H_2L^{2\text{-Et-5-Me}})_2](ClO_4)_2$ was in the HS state at room temperature. These spin states were retained in solution. X-ray structural studies revealed that the interligand steric repulsion between an ethyl group of an $H_2L^{2\text{-Et-5-Me}}$ ligand and the other ligand in $[Fe(H_2L^{2\text{-Et-5-Me}})_2]^{2+}$ is responsible for the observed change in the spin state. In this case, the steric effect outweighs the electron-donating effect of the alkyl groups.

A variety of magnetic behaviors were observed in the dinuclear complexes. For example, **2-block** stayed in the HS state at least above 50 K, while **2-plate** exhibited an abrupt spin transition, [LS–HS] ↔ [HS–HS], and the existence of the mixed-spin state [LS–HS] was confirmed from X-ray crystallographic data. The different magnetic behaviors were accounted for by the different molecular structures resulting from intermolecular interactions.

The uncoordinated NH groups of the imidazole moiety of $[Fe_2(H_2L^{2\text{-Et-5-Me}})_3]^{4+}$ can be partly deprotonated to form intermolecular N–H···N hydrogen bonds. Because the dinuclear complexes have a homochiral structure, Δ–Δ or Λ–Λ, controlled deprotonation of $[Fe_2(H_2L^{2\text{-Et-5-Me}})_3]^{4+}$ may form a homochiral SCO complex with high dimensionality. Studies along this line are in progress in our laboratories.

Experimental

Caution! Perchlorate salts of metal complexes are potentially explosive. Only small quantities of material should be prepared, and the samples should be handled with care.

Materials. All reagents and solvents used in the syntheses were of reagent grade, and they were used without further purification.

Ligand, $H_2L^{2\text{-Et-5-Me}}$. A methanol solution (10 mL) of hydrazine monohydrate (1.01 g, 20 mmol) was added to a warm methanol solution (20 mL) of 2-ethyl-4-methyl-5-formylimidazole (5.52 g, 40 mmol). The mixture was stirred at room temperature for 1 h, and a yellow precipitate was collected by filtration. Yield: 4.74 g (87%). Anal. Found: C, 61.88; H, 7.31; N, 30.95%. Calcd for $C_{14}H_{20}N_6$: C, 61.74; H, 7.40; N, 30.85%. IR (KBr disk): $\nu_{C=N}$ (imine) 1625 cm^{-1}. Crystals suitable for the X-ray structure analysis were obtained by slow evaporation of the filtrate.

$[Fe(H_2L^{2\text{-Et-5-Me}})_2](ClO_4)_2\cdot CH_3OH$ (1). $Fe(ClO_4)_2\cdot 6H_2O$ (0.363 g, 1.0 mmol) was added to a suspension of $H_2L^{2\text{-Et-5-Me}}$ (0.544 g, 2.0 mmol) in methanol (20 mL). The mixture was heated at 60 °C for 1 h. The solution was filtered, and diethyl ether (100 mL) was added to the filtrate. Red crystals that deposited on standing were collected by filtration. Yield: 0.658 g (79%). Anal. Found: C, 41.38; H, 4.97; N, 20.44%. Calcd for $C_{29}H_{44}Cl_2FeN_{12}O_9$: C, 41.89; H, 5.33; N, 20.21%. IR (KBr disk): $\nu_{C=N}$ (imine) 1634, 1559 cm^{-1}; ν_{Cl-O} (ClO_4^-) 1121 cm^{-1}. UV–vis (CH_3CN): 350 (51600), 446 nm (987 $M^{-1}\,cm^{-1}$). Crystals suitable for the X-ray structure analysis were obtained by recrystallization of the complex from methanol–diisopropyl ether.

$[Fe_2(H_2L^{2\text{-Et-5-Me}})_3](ClO_4)_4\cdot H_2O$ (2-plate′) and $[Fe_2(H_2L^{2\text{-Et-5-Me}})_3](ClO_4)_4\cdot 0.5CH_3CN$ (2-block′). $H_2L^{2\text{-Et-5-Me}}$ (0.082 g, 0.3 mmol) was added to a solution of $Fe(ClO_4)_2\cdot 6H_2O$ (0.072 g, 0.2 mmol) in acetonitrile (15 mL), and the mixture was stirred in an ice bath for 10 min. The reaction mixture was filtered to remove any undissolved substance, and diisopropyl ether (35 mL) was added to the filtrate to form a mixture of yellow plate and block crystals. Yield: 0.045 g (17%). They were separated manually. Elemental analyses were carried out after drying. Anal. (plate crystals). Found: C, 37.63; H, 4.38; N, 18.50%. Calcd for $C_{42}H_{62}Cl_4Fe_2N_{18}O_{17}$: C, 37.51; H, 4.64; N, 18.75%. Anal. (block crystals). Found: C, 38.52; H, 4.48; N, 19.09%. Calcd for $C_{43}H_{61.5}Cl_4Fe_2N_{18.5}O_{16}$: C, 38.33; H, 4.60; N, 19.23%. IR (KBr disk): $\nu_{C=N}$ (imine) 1628 cm^{-1}; ν_{Cl-O} (ClO_4^-) 1111 cm^{-1}. UV–vis (CH_3CN): 315 (59800), 460 (sh, 1100), 600 nm (sh, 70 $M^{-1}\,cm^{-1}$).

Physical Measurements. IR spectra were recorded on a JASCO FT/IR FT-550 spectrophotometer with the samples prepared as KBr disks. UV–vis absorption spectra were recorded with a JASCO Ubest-550 spectrophotometer. Magnetic susceptibilities were measured with a Quantum Design MPMS SQUID magnetometer in the 5–300 K temperature range at 2 K min^{-1} sweep rate under an applied magnetic field of 1 T. Corrections for diamagnetism were applied using Pascal's constants.

X-ray Data Collection, Reduction, and Structure Determination. The X-ray diffraction data were collected using a Rigaku RAXIS RAPID II imaging plate area detector employing graphite-monochromated Mo Kα radiation ($\lambda = 0.71073$ Å). The structures were determined by direct methods (SHELXS 97 or SIR97[14]) and expanded using Fourier techniques[15] and successive Fourier difference methods with refinement of full-matrix least-squares analysis on F^2. The nonhydrogen atoms were refined anisotropically. The hydrogen atom on the imidazole nitrogen of the ligand $H_2L^{2\text{-Et-5-Me}}$ was found from the Fourier map and its position was corrected to the ideal position. Other hydrogen atoms were introduced by calculations on the ideal positions. All hydrogen atoms were treated using the riding model. All calculations were performed using the Crystal Structure 3.8 software package.[16] Crystallographic data have been deposited with Cambridge Crystallographic Centre: Deposition numbers CCDC 538557, 538558, 538561, and 538562 for compounds, $H_2L^{2\text{-Et-5-Me}}$, **1**, **2-block**, and **2-plate**, respectively. Copies of the data can be obtained free of charge via http://www.ccdc.cam.ac.uk/conts/retrieving.html (or from the Cambridge Crystallographic Data Centre, 12, Union Road, Cambridge, CB2 1EZ, U.K.; Fax: +44 1223 336033; e-mail: deposit@ccdc.cam.ac.uk).

This work was supported by a Grant-in-Aid for Scientific Research (Nos. 16205010, 17350028, and 20550064) from the Ministry of Education, Culture, Sports, Science and Technology of Japan.

Supporting Information

Selected bond lengths and angles for $H_2L^{2\text{-Et-5-Me}}$, X-ray molecular structures of **2-block**, and crystal packing diagrams of $H_2L^{2\text{-Et-5-Me}}$, **1**, **2-block**, and **2-plate**. This material is available free of charge on the Web at: http://www.csj.jp/journals/bcsj/.

References

1 a) E. König, *Prog. Inorg. Chem.* **1987**, *35*, 527. b) E. König, *Struct. Bond.* **1991**, *76*, 51. c) H. A. Goodwin, *Coord. Chem. Rev.* **1976**, *18*, 293. d) P. Gütlich, A. Hauser, H. Spiering, *Angew. Chem., Int. Ed. Engl.* **1994**, *33*, 2024. e) J. A. Real, A. B. Gaspar, V. Niel, M. C. Muñoz, *Coord. Chem. Rev.* **2003**, *236*, 121. f) G. Lemercier, M. Verelst, A. Bousseksou, F. Varret, J.-P. Tuchagues, in *Magnetism: A Supramolecular Function*, ed. by O. Kahn, NATO ASI Series, Series C 484, Kluwer Academic Publ., Dordrecht (Pays-Bas), **1996**, p. 335. g) P. Gütlich, Y. Garcia, T. Woike, *Coord. Chem. Rev.* **2001**, *219–221*, 839. h) *Top. Curr. Chem.* **2004**, *233*. doi:10.1007/b40394-9; *Top. Curr. Chem.* **2004**, *234*. doi:10.1007/b93641; *Top. Curr. Chem.* **2004**, *235*. doi:10.1007/b96439. i) J. A. Real, A. B. Gaspar, M. C. Muñoz, *Dalton Trans.* **2005**, 2062. j) G. Vankó, F. Renz, G. Molnár, T. Neisius, S. Kárpáti, *Angew. Chem., Int. Ed.* **2007**, *46*, 5306. k) A. Bousseksou, N. Negre, M. Goiran, L. Salmon, J.-P. Tuchagues, M.-L. Boillot, K. Boukheddaden, F. Varret, *Eur. Phys. J. B* **2000**, *13*, 451.

2 a) O. Kahn, C. J. Martinez, *Science* **1998**, *279*, 44. b) S. Hayami, K. Danjobara, K. Inoue, Y. Ogawa, N. Matsumoto, Y. Maeda, *Adv. Mater.* **2004**, *16*, 869. c) J. F. Létard, P. Guionneau, L. Goux-Capes, *Top. Curr. Chem.* **2004**, *235*, 221. d) V. Niel, J. M. Martinez-Agudo, M. C. Muñoz, A. B. Gaspar, J. A. Real, *Inorg. Chem.* **2001**, *40*, 3838.

3 a) W. J. Stratton, D. H. Busch, *J. Am. Chem. Soc.* **1958**, *80*, 1286. b) W. J. Stratton, D. H. Busch, *J. Am. Chem. Soc.* **1958**, *80*, 3191. c) W. J. Stratton, D. H. Busch, *J. Am. Chem. Soc.* **1960**, *82*, 4834.

4 a) Y. Sunatsuki, M. Sakata, S. Matsuzaki, N. Matsumoto, M. Kojima, *Chem. Lett.* **2001**, 1254. b) Y. Sunatsuki, Y. Ikuta, N. Matsumoto, H. Ohta, M. Kojima, S. Iijima, S. Hayami, Y. Maeda, S. Kaizaki, F. Dahan, J.-P. Tuchagues, *Angew. Chem., Int. Ed.* **2003**, *42*, 1614. c) H. Ohta, Y. Sunatsuki, Y. Ikuta, N. Matsumoto, S. Iijima, H. Akashi, T. Kambe, M. Kojima, *Mater. Sci.* **2003**, *21*, 191. d) Y. Ikuta, M. Ooidemizu, Y. Yamahata, M. Yamada, S. Osa, N. Matsumoto, S. Iijima, Y. Sunatsuki, M. Kojima, F. Dahan, J.-P. Tuchagues, *Inorg. Chem.* **2003**, *42*, 7001. e) M. Yamada, M. Ooidemizu, Y. Ikuta, S. Osa, N. Matsumoto, S. Iijima, M. Kojima, F. Dahan, J.-P. Tuchagues, *Inorg. Chem.* **2003**, *42*, 8406. f) Y. Sunatsuki, H. Ohta, M. Kojima, Y. Ikuta, Y. Goto, N. Matsumoto, S. Iijima, H. Akashi, S. Kaizaki, F. Dahan, J.-P. Tuchagues, *Inorg.*

Chem. **2004**, *43*, 4154. g) H. Ohta, Y. Sunatsuki, M. Kojima, S. Iijima, H. Akashi, N. Matsumoto, *Chem. Lett.* **2004**, *33*, 350. h) M. Yamada, E. Fukumoto, M. Ooidemizu, N. Bréfuel, N. Matsumoto, S. Iijima, M. Kojima, N. Re, F. Dahan, J.-P. Tuchagues, *Inorg. Chem.* **2005**, *44*, 6967. i) M. Yamada, H. Hagiwara, H. Torigoe, N. Matsumoto, M. Kojima, F. Dahan, J.-P. Tuchagues, N. Re, S. Iijima, *Chem.—Eur. J.* **2006**, *12*, 4536. j) S. Iijima, F. Mizutani, O. Niwa, N. Matsumoto, Y. Sunatsuki, M. Kojima, *Hyperfine Interact.* **2005**, *166*, 397.

5 a) K. Fujita, R. Kawamoto, R. Tsubouchi, Y. Sunatsuki, M. Kojima, S. Iijima, N. Matsumoto, *Chem. Lett.* **2007**, *36*, 1284. b) R. Kawamoto, K. Fujita, H. Maruyama, Y. Sunatsuki, T. Suzuki, H. Ishida, M. Kojima, S. Iijima, N. Matsumoto, *Inorg. Chem.* **2009**, *48*, 8784.

6 K. Nakamoto, *Infrared and Raman Spectra of Inorganic and Coordination Compounds, Part B*, 5th ed., John Wiley & Sons, New York, **1997**.

7 N. M. Levy, M. C. Laranjeira, A. Neves, C. V. Franco, *J. Coord. Chem.* **1996**, *38*, 259.

8 L. A. Saghatforoush, A. Aminkhani, S. Ershad, G. Karimnezhad, S. Ghammamy, R. Kabiri, *Molecules* **2008**, *13*, 804.

9 M. A. Hoselton, L. J. Wilson, R. S. Drago, *J. Am. Chem. Soc.* **1975**, *97*, 1722.

10 a) For example: Y. Garcia, C. M. Grunert, S. Reiman, O. van Campenhoudt, P. Gütlich, *Eur. J. Inorg. Chem.* **2006**, 3333. b) K. Yoneda, K. Adachi, S. Hayami, Y. Maeda, M. Katada, A. Fuyuhiro, S. Kawata, S. Kaizaki, *Chem. Commun.* **2006**, 45.

11 a) V. Ksenofontov, A. B. Gaspar, V. Niel, S. Reiman, J. A. Real, P. Gütlich, *Chem.—Eur. J.* **2004**, *10*, 1291. b) N. Ortega-Villar, A. L. Thompson, M. C. Muñoz, V. M. Ugalde-Saldívar, A. E. Goeta, R. Moreno-Esparza, J. A. Real, *Chem.—Eur. J.* **2005**, *11*, 5721. c) R. Kitashima, S. Imatomi, M. Yamada, N. Matsumoto, Y. Maeda, *Chem. Lett.* **2005**, *34*, 1388. d) J. A. Real, H. Bolvin, A. Bousseksou, A. Dworkin, O. Kahn, F. Varret, J. Zarembowitch, *J. Am. Chem. Soc.* **1992**, *114*, 4650. e) V. Ksenofontov, H. Spiering, S. Reiman, Y. Garcia, A. B. Gaspar, N. Moliner, J. A. Real, P. Gütlich, *Chem. Phys. Lett.* **2001**, *348*, 381. f) K. Nakano, S. Kawata, K. Yoneda, A. Fuyuhiro, T. Yagi, S. Nasu, S. Morimoto, S. Kaizaki, *Chem. Commun.* **2004**, 2892. g) J. J. Amoore, C. J. Kepert, J. D. Cashion, B. Moubaraki, S. M. Neville, K. S. Murray, *Chem.—Eur. J.* **2006**, *12*, 8220. h) M. Ruben, U. Ziener, J.-M. Lehn, V. Ksenofontov, P. Gütlich, G. B. M. Vaughan, *Chem.—Eur. J.* **2005**, *11*, 94. i) M. Ruben, J. Rojo, F. J. Romero-Salguero, L. H. Uppadine, J.-M. Lehn, *Angew. Chem., Int. Ed.* **2004**, *43*, 3644.

12 M. Klingele, B. Moubaraki, J. D. Cashion, K. S. Murray, S. Brooker, *Chem. Commun.* **2005**, 987.

13 J. K. Beattie, *Adv. Inorg. Chem.* **1988**, *32*, 1.

14 G. M. Sheldrick, *SHELXS97*, University of Göttingen, Germany, **1997**; SIR97: A. Altomare, M. C. Burla, A. G. G. Moliterni, G. Polidori, R. Spagna, *J. Appl. Crystallogr.* **1999**, *32*, 115.

15 DIRDIF99: P. T. Beurskens, G. Admiraal, G. Beurskens, W. P. Bosman, de R. Gelder, R. Israel, J. M. M. Smits, *DIRDIF-99 Program System, Technical Report of the Crystallography Laboratory*, University of Nijmegen, The Netherlands, **1999**.

16 *CrystalStructure 3.8; Crystal Structure Analysis Package*, Rigaku and Rigaku/MSC, The Woodlands, TX, USA, **2001**–**2007**.